Supporting Information

Enhancing cyclic stability of hollow architecture Li-rich cathode via Ce integrated surface/interface/doping engineering

1. Experimental Section

1.1 Materials preparation.

The $Mn_{0.75}Ni_{0.25}CO_3$ precursor was synthesized via using a carbonate coprecipitation method. The mixed solution (2 mol L^{-1}) containing a molar ratio of Mn:Ni =3:1 of $MnSO_4 \cdot H_2O$ and $NiSO_4 \cdot 6H_2O$ was pumped into a continuously stirred tank reactor (3 L) under inertial N_2 atmosphere. Then, 2 mol $L^{-1}$of Na_2CO_3 solution and 0.1 mol L^{-1} of $NH_3 \cdot H_2O$ were added in sequence into the tank reactor. The temperature (55 °C), pH value (7.8), and stirring speed (1000 rpm) of the solution were carefully controlled and maintained constant. The precursor powders were obtained through washing, filtering, and drying in a vacuum oven for 6h to remove adsorbed water.

LLO samples were prepared by mixing $Mn_{0.75}Ni_{0.25}CO_3$ precursors and Li_2CO_3 at the molar ratio of Li: TM=1.05 (Li excess 5%). After calcining at 850 °C for 12 h, the samples were cooled to 500℃ and then sintered at 500℃ for 5 hours in air atmosphere. LLO@Ce samples were prepared by homogeneously mixing $Mn_{0.75}Ni_{0.25}CO_3$ precursors, Li_2CO_3 and CeO_2 in the molar ratio of Li:TM:Ce=1.05:1:0.005, and then sintering according to the above process. For the synthesis of LLO@Ce-LCO, the LLO@Ce and $Ce(NO_3)_3 \cdot 6H_2O$ were mixed in ethanol solution with the molar ration of TM: Ce=1: 0.005, the desired powder materials were obtained by evaporation by stirring at 80℃ and then calcining at 600°C for 10 h in air atmosphere. The synthesis process is shown in Fig. 1a.

1.2 Characterization methods.

X-ray diffraction (XRD) was used to detect the details of the crystal phase. The data was collected in a scan speed of 3° min^{-1} with Cu Kα radiation. Refine treatment was performed by Full Prof Suite software. X-ray photoelectron spectroscopy (XPS)

spectrum was obtained by a spectrometer of Kratos Analytical Ltd. with Al Kαradiation. The spectrum data was fitted with XPS Peak-Fit software. Scanning electron microscopy (SEM) and transmission electron microscopy (TEM) were used to evaluate the morphology or microstructure of the materials. Energy dispersive X-ray spectroscopy (EDS) mapping images were obtained by SEM. The fast Fourier transform (FFT) images were obtained via Digital-Micrograph software.

1.3 Electrochemical Measurements.

To investigate the electrochemical performance of the materials, the cell in a coin configuration (CR2016) was assembled with the cathode, separator, lithium plate, and electrolyte under an Ar atmosphere. The electrode was prepared by casting the slurry composing cathode material, carbon black, and binder (80:10:10 by weight) on the Al foil. The loading mass of the active material was fixed at 1.0 ± 0.1 mg to ensure the veracity of measurement results. Li metal was the counter and reference electrode. Celgard 2400 was used as separator. The electrolyte was 1M $LiPF_6$ in ethylene carbonate/dimethyl carbonate, (1:1 by volume). The as-prepared cells were subjected to electrochemical measurements via Neware software. The cyclic voltammetry (CV) tests were carried out between 2.0 and 4.8 V. A galvanostatic intermittent titration technique (GITT) was conducted to evaluate the kinetic properties of electrodes. AC impedance spectrum (0.01-10^5 Hz) were measured using a multichannel potentiostat galvanostat from Princeton Applied Research.

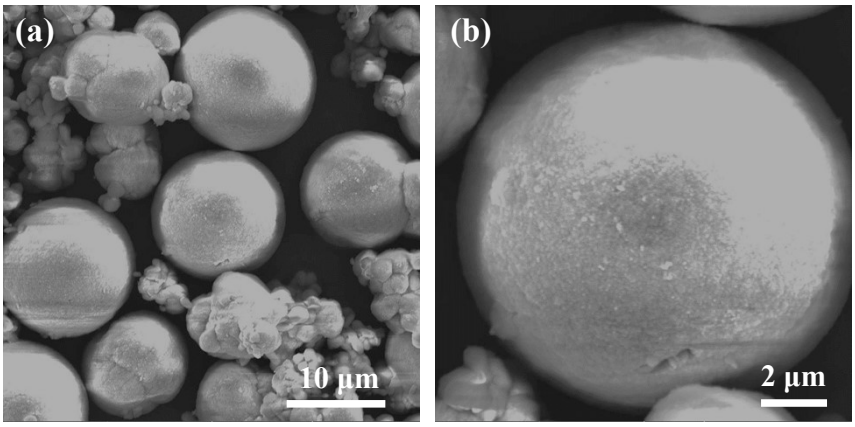

Fig. S1 The carbonate precursor in different magnifications

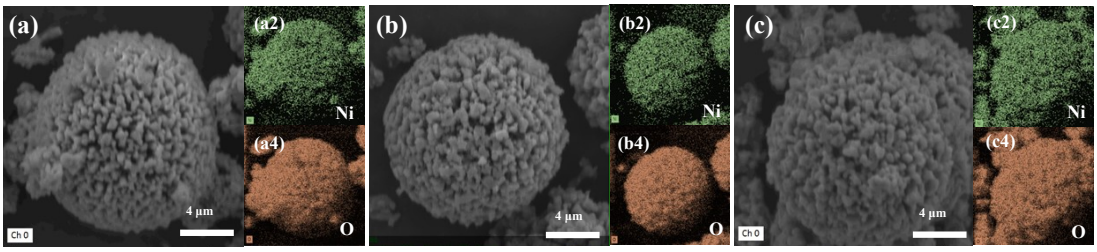

Fig. S2. (a-c) Elemental mapping of three samples

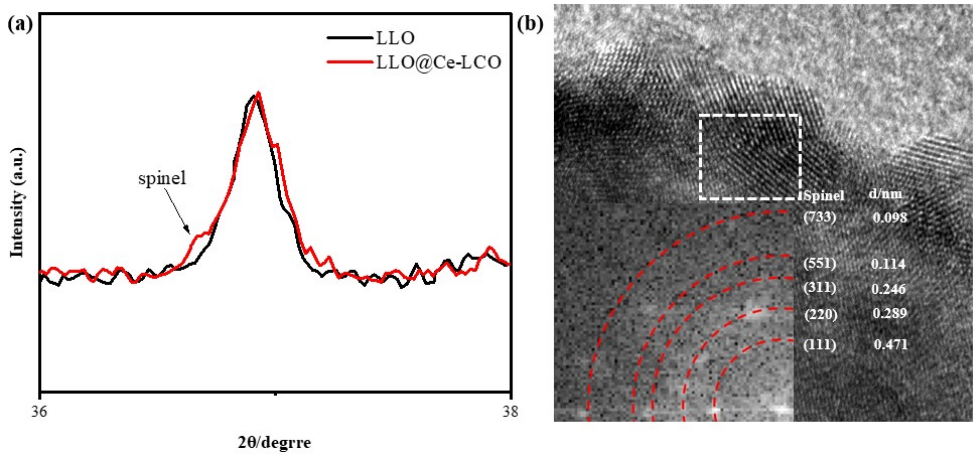

Fig. S3. (a) The XRD comparison of two samples and (b) the fast Fourier transform (FFT) of spinel structure.

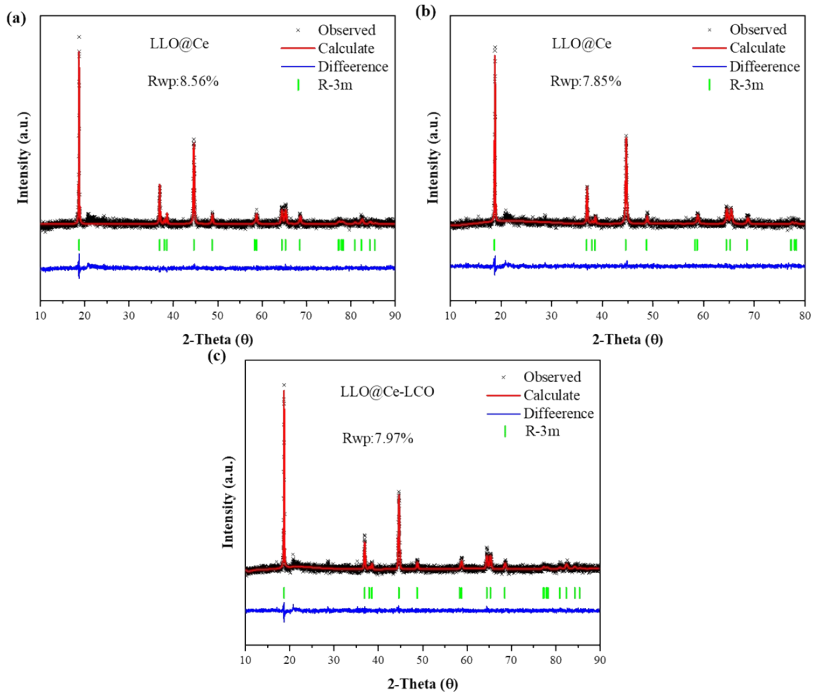

Fig. S4. Rietveld refinement images of a) LLO, b) LLO@Ce, c) LLO@Ce-LCO

Table S1. The refined crystallographic parameters of the as prepared samples.

material	a=b (Å)	c (Å)	alpha	beta	gamma	volume(Å^3)
LLO	2.855349	14.23645	90	90	120	100.52
LLO@Ce	2.854878	14.23972	90	90	120	100.51
LLO@Ce-LCO	2.860844	14.25423	90	90	120	101.033

Table S2. The refined crystallographic parameters of the as prepared samples.

label	x	y	z	frac
		LLO		
Li1	0	0	0	0.975
Co1	0	0	0.5	0.333
Ni2	0	0	0	0.025
Mn1	0	0	0.5	0.333
Ni1	0	0	0.5	0.309
Li2	0	0	0.5	0.025
O1	0	0	0.2411	1
		LLO@Ce		
Li1	0	0	0	0.975
Co1	0	0	0.5	0.332
Ni2	0	0	0	0.025
Mn1	0	0	0.5	0.330
Ni1	0	0	0.5	0.308
Li2	0	0	0.5	0.025
O1	0	0	0.2411	1
Ce8	0	0	0.5	0.005
		LLO@Ce-LCO		
Li1	0	0	0	0.975
Co1	0	0	0.5	0.332
Ni2	0	0	0	0.025
Mn1	0	0	0.5	0.328
Ni1	0	0	0.5	0.305
Li2	0	0	0.5	0.025
O1	0	0	0.2411	1
Ce8	0	0	0.5	0.005
Ce9	0	0	0.5	0.005

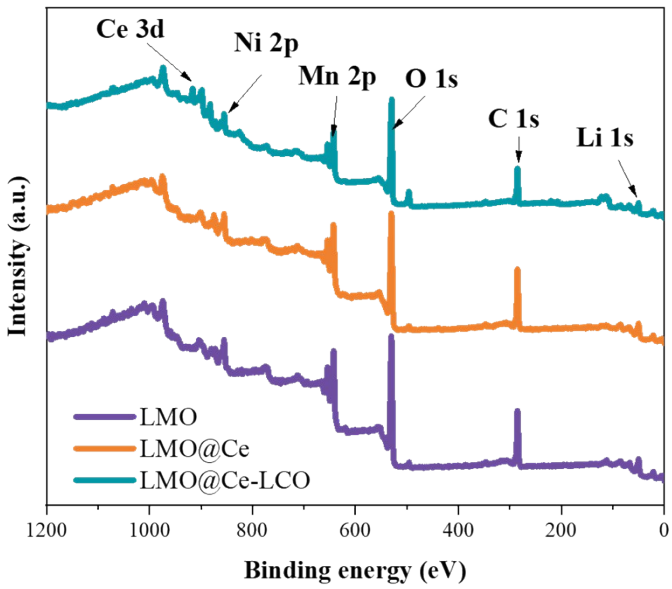

Fig. S5. XPS patterns of the LLO, LLO@Ce and LLO@Ce-LCO samples.

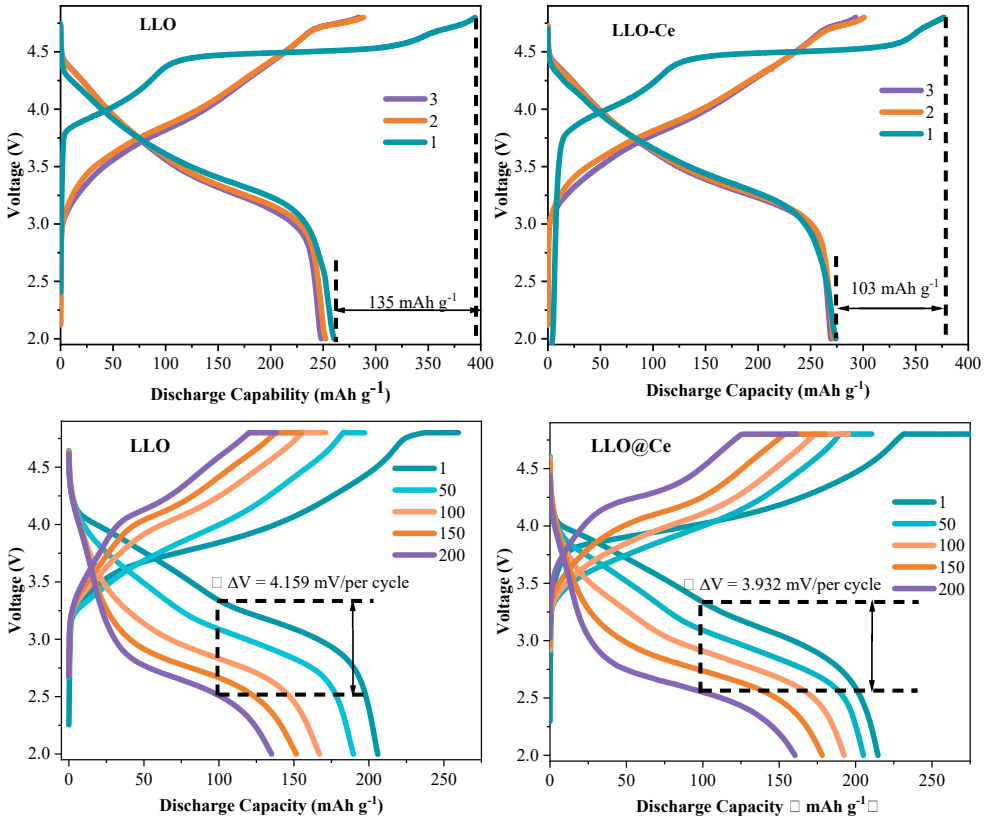

Fig. S6. a-b) Initial charging/discharging profiles of the samples at 0.1 C. c-d) The selected differential capacity versus voltage curves of the samples at 1 C.

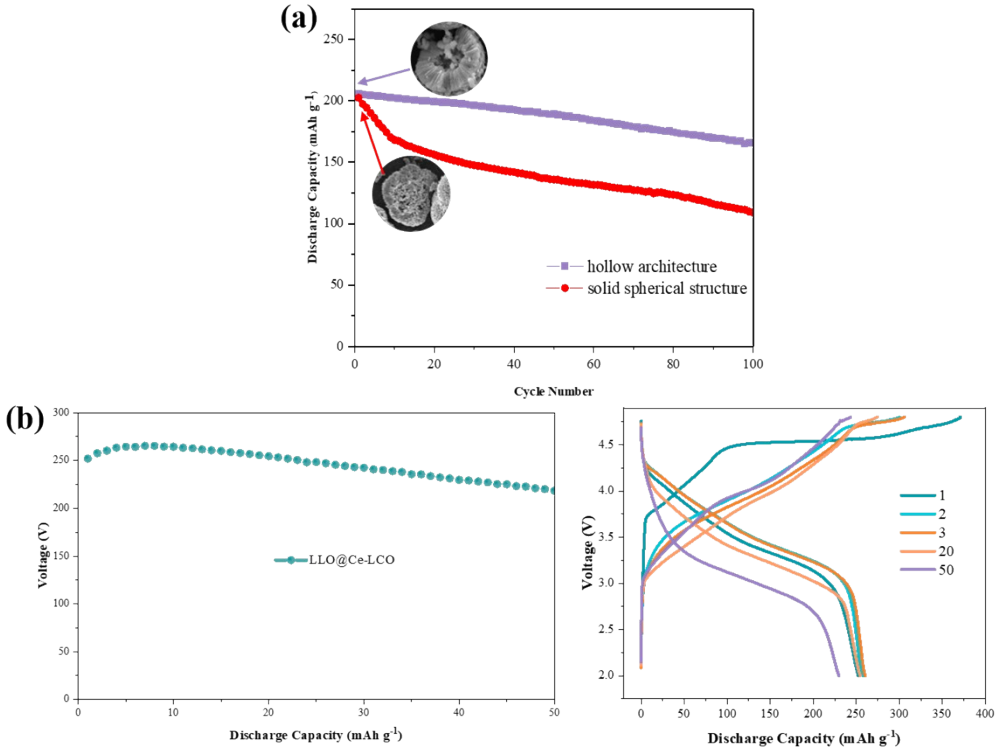

Fig. S7. (a) The comparison of electrical properties of Li-rich materials with hollow and solid structures, (b) Cyclic performance and (c) charge-discharge curves of LLO@Ce-LCO at 0.2C

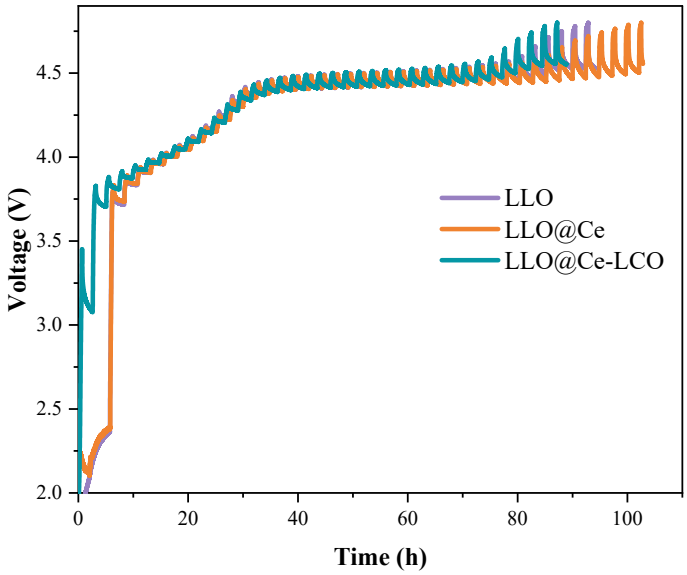

Fig. S8. GITT curve of three samples.

Li-ion diffusivity (D_{Li^+}) is identified by GITT. D_{Li^+} was analyzed by the

following simplified equation according to Fick's second law.

$$D_{Li^+} = \frac{4}{\pi\tau}\left(\frac{m_B V_m}{M_B S}\right)^2\left(\frac{\Delta E_s}{\Delta E_t}\right)^2$$

Where τ is current pulse duration, m_B and M_B are the active mass and molar mass, V_m is the molar volume; and S is interface area between electrode and electrolyte, ΔE_s is voltage change between the open circuit voltage measured at the end of two consecutive measurements, ΔE_t is total voltage change during charging or discharging.

D_{Li^+} calculation of LLO, LLO@Ce and LLO@Ce-LCO electrodes is shown in Fig. 4(j-l). By comparison, it is found that the Li^+ diffusion coefficient of LLO material is the lowest, around 10^{-11} cm^2 s^{-1}. The Li^+ diffusion coefficient of LLO@Ce sample is improved to some extent, but still lower than 10^{-10} cm^2 s^{-1}. However, the Li^+ diffusion coefficient of LLO@Ce-LCO is significantly higher than 10^{-10} cm^2 s^{-1}. The reason for this effect may be that Ce ions are inserted into the lattice, it can expand the c-axis spacing, which is conducive to the inhibition of anionic oxygen precipitation and the acceleration of lithium ions transmission rate. While the external oxygen storage layer is constructed, the subsurface spinel structure constructs the three-dimensional conductive network of lithium ions, which accelerates the transmission of lithium ion.

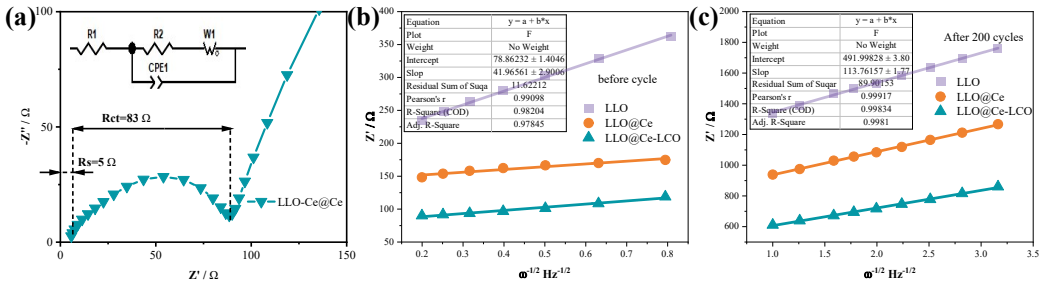

Fig. S9. (a) Impedance of LLO@Ce-LCO sample before cycling. (b, c) Warburg diffusion coefficients of three samples and the slop of LLO@Ce-LCO sample.

The D_{Li^+} were calculated by the following equation:

$$D_{Li^+} = \frac{R^2T^2}{2A^2n^4F^4C^2\sigma^2}$$

(1)

$$Z^{'} = R_{\Omega} + R_{ct} + \sigma \cdot \omega^{-0.5} \quad (2)$$

Where R represents the Gas constant; T is the thermodynamic temperature; A stands for the superficial area of the electrode; n is the quantity of the electrons in the electronic transfer process; F represents the Faraday's constant; C is the concentration of Li^{+} ions; σ is the Warburg factor which fitted in the Fig. S8, according to the equation (2).

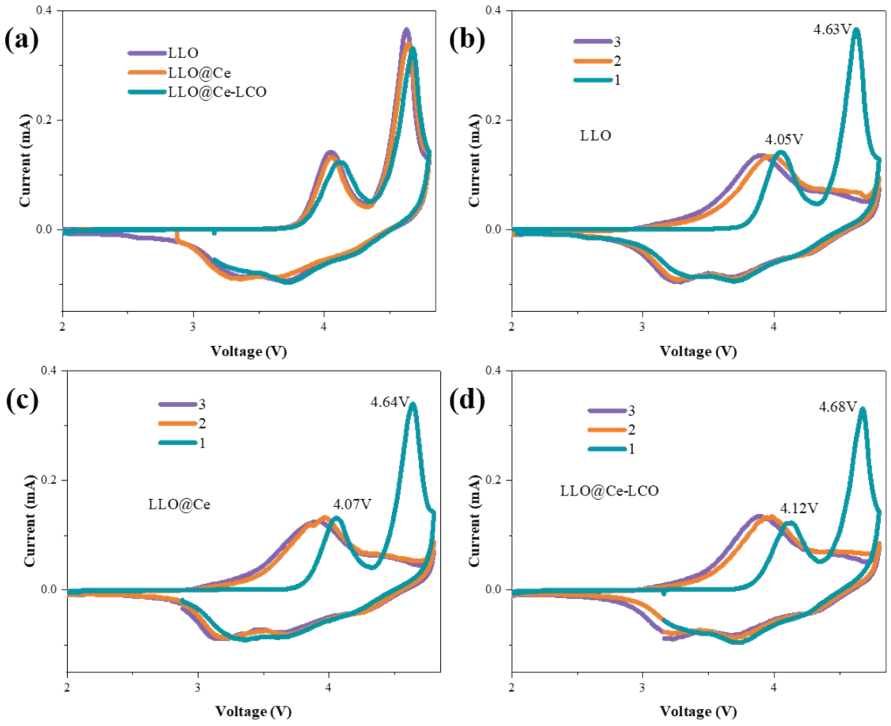

Fig. S10. a) Comparison of CV curves of the first cycle of the three samples. b-d) The CV curves of the first three cycles of the three samples, respectively.

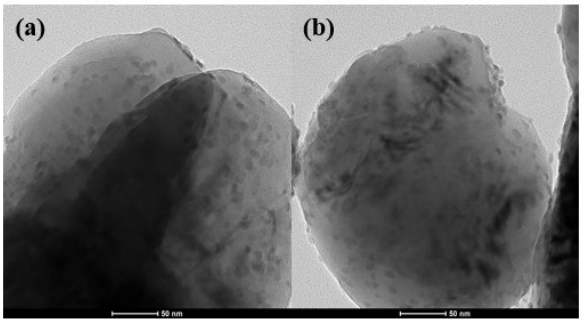

Fig. S11. (a) and (b) TEM images of LLO@Ce-LCO sample.

Table S3. A brief summary of the electrochemical performance of LLO cathode in this work and those reported in literatures

Ref.	Modification method	Initial discharge capacity (mAh g^{-1})	Capacity retention
This work	Three in one design	268 (0.1 C)	94% (1 C,100 cycles) 86% (1 C,200 cycles)
[10]	Ce surface coating	265 (0.1 C)	81% (1 C,200 cycles)
[12]	La surface coating and doping	280 (0.1 C)	92.8% (1 C,100 cycles)
[13]	LiF gradient doping	267 (0.1 C)	82% (0.5 C,20 cycles)
[17]	Co_xO_y surface coating	260 (0.1 C)	82% (0.5 C,200 cycles)
[25]	Hollowspheres design	267 (0.1 C)	80.0% (1 C,100 cycles)
[26]	Hollowspheres design	261 (0.12 C)	74% (1 C,100 cycles)
[28]	Na doping	276 (0.1 C)	80.% (1 C,200 cycles)

Table S4. The simulation values of R_S, R_{ct} and D^{Li+} for the LLO, LLO@Ce and LLO@Ce-LCO

samples	R_1 (Ω)	R_2 (Ω)	D^{Li+} (cm^2 s^{-1})
LLO	1.57	152.7	2.98×10^{-12}
LLO@Ce	1.46	166.9	6.49×10^{-12}
LLO@Ce-LCO	1.28	99.4	2.12×10^{-11}